In Vivo Imaging

International Edition: DOI: 10.1002/anie.201507868
German Edition: DOI: 10.1002/ange.201507868

High-contrast Noninvasive Imaging of Kidney Clearance Kinetics Enabled by Renal Clearable Nanofluorophores

*Mengxiao Yu, Jinbin Liu, Xuhui Ning, and Jie Zheng**

Abstract: *Noninvasive imaging of kidney clearance kinetics (KCK) of renal clearable probes is key to studying unilateral kidney function diseases, but such imaging is highly challenging to achieve with in vivo fluorescence. While this long-standing challenge is often attributed to the limited light penetration depth, we found that rapid and persistent accumulation of conventional dyes in the skin "shadowed" real fluorescence signals from the kidneys and prevented noninvasive imaging of KCK, which, however, can be addressed with renal clearable nanofluorophores. By integrating near infrared emission with efficient renal clearance and ultralow background interference, the nanofluorophores can increase kidney-contrast enhancement and imaging-time window by approximately 50- and 1000-fold over conventional dyes, and significantly minimize deviation between noninvasive and invasive KCK, laying down a foundation for translating in vivo fluorescence imaging in preclinical noninvasive kidney function assessments.*

Noninvasive assessment of single kidney function is a key approach for understanding unilateral kidney diseases that are affecting a large population of adults worldwide.[1] Noninvasive imaging of kidney clearance kinetics (KCK) of renal clearable probes is an essential tool to quantify individual kidney function.[2] Since accurate evaluation of kidney function requires dynamic imaging of kidneys at high contrast and high temporal resolution, nuclear imaging,[2a] magnetic resonance imaging (MRI),[2b] and computed tomography (CT)[2c] currently are the major tools for both clinical diagnosis and preclinical kidney function studies. However, because of high cost, limited access, and potential radiation exposure of current radiology-based kidney functional imaging, low-cost and high-sensitivity kidney functional imaging tools are highly desired for preclinical kidney research.[3]

In vivo near-infrared (NIR) fluorescence imaging has been widely used in preclinical disease studies owing to its low cost, high sensitivity, and no risk of radiation exposure.[4] Because of these merits, fluorescence imaging has also been translated into clinical practice to improve surgical accuracy[4a,5] and minimize potential damage to healthy tissues.[6] However, translation of fluorescence techniques into noninvasive preclinical kidney functional imaging remains highly challenging because very few fluorescent contrast agents can noninvasively report KCK.

Herein, we report that this long-standing challenge in noninvasive fluorescence imaging of KCK is not due to the limited penetration of light, but rapid and persistent accumulation of conventional fluorophores in the skin tissues after intravenous (iv) injection. Owing to their high lipophilicity, conventional organic fluorophores tend to accumulate in the skin lipid membranes.[7a,b] Amphiphilic fluorescent NPs such as quantum dots,[7c] dye-conjugated silica NPs,[7a] and nonluminescent plasmonic AuNPs[7c] also have high accumulation in the skin. Although skin accumulation of organic dyes and amphiphilic NPs are offering exciting opportunities for detection of skin diseases,[7c,8] such high accumulation of the fluorophores in the skin background is a roadblock for accurate quantification of KCK.

This challenge can be readily addressed with a renal clearable inorganic nanofluorophore, NIR-emitting glutathione-coated gold nanoparticle (GS-AuNP), which integrates deep tissue-penetration of NIR light with desired in vivo behaviors of contrast agents to synergistically achieve high-contrast noninvasive fluorescence kidney imaging. More importantly, with assistance of GS-AuNPs, the kidney time-fluorescence intensity curves (TFICs) obtained from noninvasive florescence imaging can report the clearance kinetics of the GS-AuNPs through the kidney, laying down a foundation for future noninvasive fluorescence kidney functional imaging.

While the low contrast enhancement in noninvasive fluorescence kidney imaging is often attributed to the limited tissue penetration of the light,[9] a comparison of kidney imaging in the visible region and NIR window revealed that light penetration depth is not the only factor that governs kidney-contrast enhancements. Figure 1 shows fluorescence images of mice injected with two Cyanine dyes, Cy3 and Cy7 (Figure 1 A,B; Supporting Information, Figure S1). While Cy3 rapidly accumulated in the kidneys within 1 min post injection (p.i.), as shown in the invasive image (Figures 1 C, S2, S3), Cy3 failed to enhance the kidney contrast noninvasively (Figure 1 D). On the other hand, NIR-emitting Cy7 only transiently enhanced kidney contrast for less than 10 min (Figure 1 F). At 10 min p.i., the kidney became undetectable noninvasively, even though Cy7 remained in the kidneys, as shown in the invasive image (Figures 1 E, S3). Quantitative analysis shows that the Cy7 has even longer skin retention time than Cy3 (Figure 1 G), implying the enhanced hydrophobicity of NIR dyes significantly increased the affinity of the molecules to tissues, consistent with previous findings.[10]

The renal-clearable fluorophore IRDye 800CW also only transiently illuminated the kidneys noninvasively for less than

[*] Dr. M. X. Yu, Dr. J. B. Liu, X. H. Ning, Prof. Dr. J. Zheng
Department of Chemistry, The University of Texas at Dallas
800 W. Campbell Rd., Richardson, TX 75080 (USA)
E-mail: jiezheng@utdallas.edu

Supporting information for this article is available on the WWW under http://dx.doi.org/10.1002/anie.201507868.

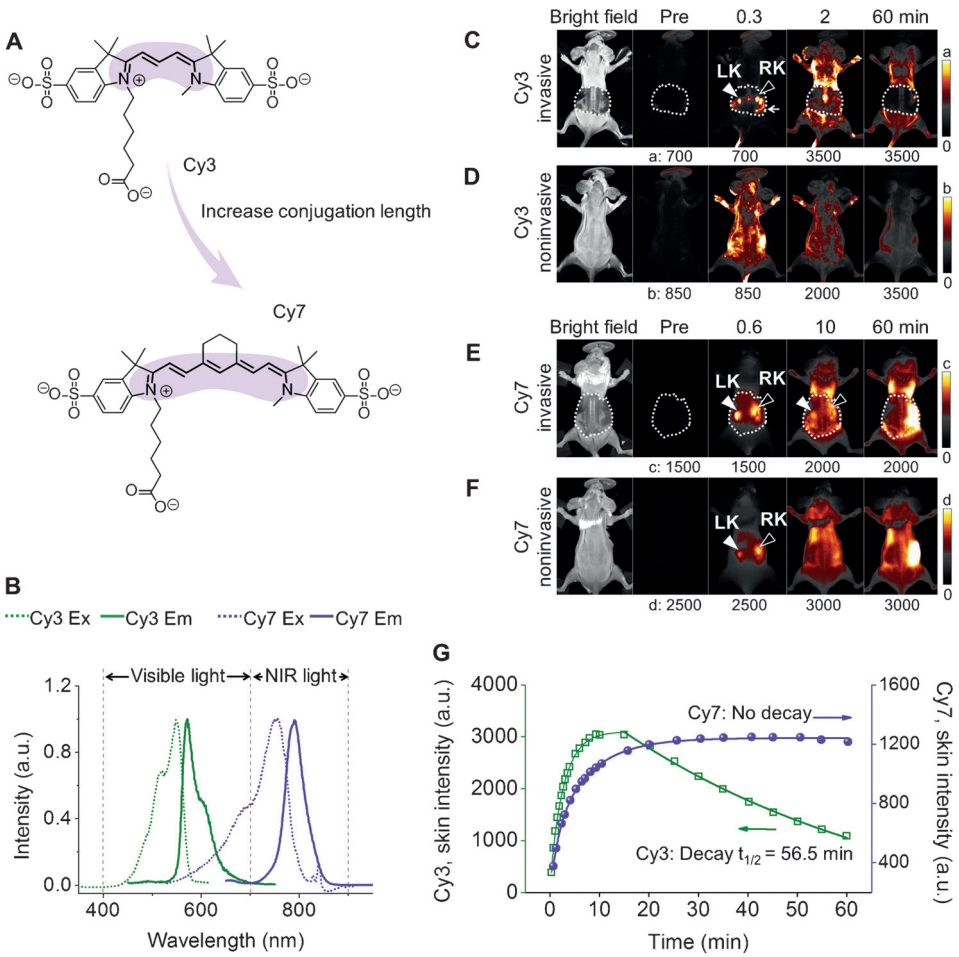

Figure 1. Fluorescence kidney imaging of mice after intravenous (iv) injection of visible-emitting Cy3 and NIR-emitting Cy7 dyes. A) Chemical structures of Cy3 and Cy7. B) Excitation and emission spectra of Cy3 and Cy7. The increase in conjugation length (highlighted in color) results in a red shift in excitation and emission maxima from the visible region (Cy3, 550/570 nm) to the NIR-optical window (Cy7, 754/790 nm). C–F) Whole-body invasive (C, E) and noninvasive (D, F) fluorescence images of mice before and after iv injection of Cy3 (C, D; Ex/Em filters: 550/600 nm) and Cy7 (E, F; Ex/Em filters: 710/790 nm). In C and E, the left and right kidneys (LK, RK) were exposed by partially removing the back skin (marked by dashed white line). G) Time-dependent fluorescence intensities of the mouse skin following dye injection.

5 min with 710 nm excitation and 790 nm emission filters (Figures 2A, B, S4). IRDye 800CW also exhibited persistent accumulation in the skin and rapid kidney clearance, which is independent of detection windows (790 nm vs. 830 nm; Figure S5), indicating that the fluorescence images truly reflect behaviors of IRDye 800CW in vivo. Quantitative studies on the contrast enhancements show that the percentages of kidney-contrast enhancement ([(mean intensity of kidney/mean intensity of surrounding tissue)−1] × 100%) increased to 67.6 ± 7.1% and 49.9 ± 9.0% for left kidney (LK) and right kidney (RK) at 0.6 min p.i., respectively, then rapidly dropped to 0 at ca. 12 min p.i. following single-exponential decay kinetics (Figure 2C). The decrease half-lives ($t_{1/2}$) of kidney-contrast enhancements of noninvasive imaging were 4.2 min and 4.5 min for LK and RK respectively, comparable to increasing signal intensity in the skin ($t_{1/2}$ = 4.1 min; Figure 2C), but faster than the dye-clearance $t_{1/2}$ (4.3 min (50.1%)/28.0 min (49.9%) and 4.7 min (46.0%)/18.9 min (54.0%) for LK and RK, respectively) obtained from invasive imaging (Figure 2D). Because of the strong skin interference, the noninvasive time-dependent fluorescence intensities of kidney areas remained at a high level 0–60 min p.i., and failed to report the actual process of dye uptake and clearance from the kidney, as seen by invasive imaging (Figure 2D). These results further confirmed that rapid accumulation and long retention of conventional organic fluorophores in the skin is a general cause for their failure in noninvasive kidney imaging. As a result, conventional organic fluorophores for noninvasive imaging of KCK face a dilemma: while increasing conjugation length shifts the excitation and emission maxima from the visible region to the NIR optical window, the large hydrophobic π-conjugated systems of NIR dyes lead to a high skin accumulation and thus generate a strong persistent fluorescence background, preventing noninvasive fluorescence imaging of KCK (Figures 2D, S6).

Unlike organic fluorophores, luminescent inorganic nanoparticles can exhibit NIR emissions owing to quantum size effects, without sacrificing their hydrophilicity.[11] Among those known renal-clearable inorganic nanoparticles,[12] luminescent GS-AuNPs (Figures 2E, S7, S8) are a class of ultrasmall inorganic nanofluorophores that can be efficiently excreted through the kidney,[13] exhibit intrinsic NIR emission without conjugation of dyes,[14] have a hydrophilic surface,[15] and show faster clearance from normal tissues than dye molecules.[16]

In contrast to organic dyes, NIR-emitting GS-AuNPs can substantially enhance kidney contrast and extend the noninvasive detection time window. The noninvasive kidney images obtained with GS-AuNPs were very similar to the invasive ones (Figure 2F). Right after injection of GS-AuNPs, the percentages of kidney contrast enhancement reached 90–150% within 12 min p.i., and gradually increased to maximum values of 240.0 ± 55.3% and 223.2 ± 41.5% for LK and RK at 60 min p.i. respectively, which were approximately 50-times higher than those obtained with IRDye 800 CW at 60 min p.i. (−4.7 ± 0.8% and −4.8 ± 5.1% for LK and RK; Figure 2G).

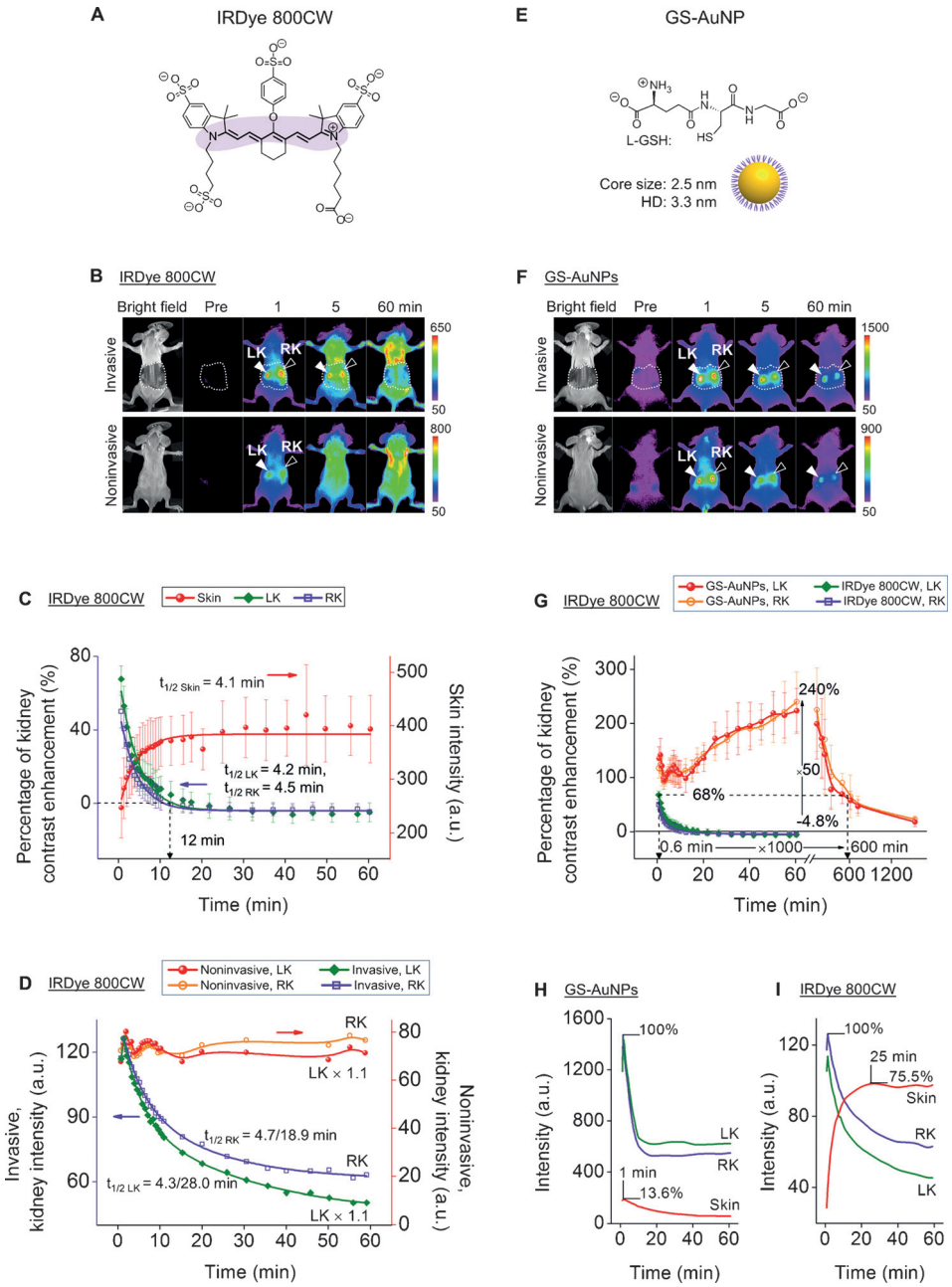

Figure 2. Comparison of renal-clearable NIR-emitting IRDye 800CW and GS-AuNPs in noninvasive kidney imaging. A) Chemical structure of IRDye 800CW. B) Whole-body invasive and noninvasive fluorescence images of mice before and after iv injection of IRDye 800CW (Ex/Em filters: 710/790 nm). The skin-removed areas were marked by dashed white line. LK, left kidney; RK, right kidney. C) Time-course changes in skin intensity and percentage of kidney-contrast enhancements of mice after iv Injection of IRDye 800CW. $N = 3$, mean ± s.d. D) Time-fluorescence intensity curves (TFICs) of kidneys obtained from noninvasive and invasive fluorescence imaging of mice after iv injection of IRDye 800CW. E) Representation of GS-AuNPs. F) Whole-body invasive and noninvasive fluorescence images of mice before and after iv injection of GS-AuNPs (Ex/Em filters: 710/830 nm). G) Comparison of time-dependent kidney contrast enhancements in percentage after GS-AuNPs and IRDye 800CW injection, respectively. $N = 3$, mean ± s.d. H, I) TFICs of kidneys and skin obtained from invasive imaging after iv injection of GS-AuNPs (H) and IRDye 800CW (I).

The kidneys remained detectable at 10 h p.i with a contrast enhancement of ca. 68% (Figure S9), which is the maximum enhancement that IRDye 800 can reach at 0.6 min p.i. (Figure 2G, green and purple), suggesting the detection time window of GS-AuNPs was ca. 1000 times longer than that of IRDye 800CW.

The dramatic improvement in kidney contrast and detection time was attributed to the low skin accumulation of the hydrophilic GS-AuNPs and subsequent rapid clearance from the skin through the kidney. The maximum intensity of skin after GS-AuNPs injection was only 13.6% of the maximum kidney intensity (Figure 2H), much lower than the skin-to-kidney ratios of Cy7 (95.3%; Figure S3) and IRDye 800CW (75.5%; Figure 2I). Furthermore, accumulation in and clearance from skin of GS-AuNPs were much faster than those of NIR organic dyes. The skin intensity after GS-AuNPs injection (Figure 2H) reached its maximum value at as early as ca. 1 min p.i., 20–30 times earlier than those of Cy7 (35 min p. i.; Figure S3) and IRDye 800CW (25 min p. i.; Figure 2I), and then immediately decreased and followed a single-exponential decay function with a $t_{1/2}$ of 12.6 min. Therefore, the interference from the skin fluorescence on kidney imaging was incredibly reduced.

Besides low skin affinity, the prolonged detection time window of the kidneys was also contributed from the long retention of GS-AuNPs in the blood because blood flow to the two kidneys is normally ca. 22% of cardiac output,[17] and renal vascular supply is up to 47% of the kidneys.[6a] The elimination half-life ($t_{1/2\beta}$) of GS-AuNPs (8.5 ± 2.1 h) was 9-times longer than that of IRDye 800CW (0.98 ± 0.08 h), which is responsible for the detection of kidneys for 10 h after injection of GS-AuNPs (Figure S9).[16]

To determine whether the kidney TFICs obtained noninvasively can truly report the clearance kinetics of the GS-AuNPs through the kidney, we quantitatively compared the kidney TFICs measured noninvasively and invasively from the same group of mice ($N = 6$). The noninvasive kidney TFIC

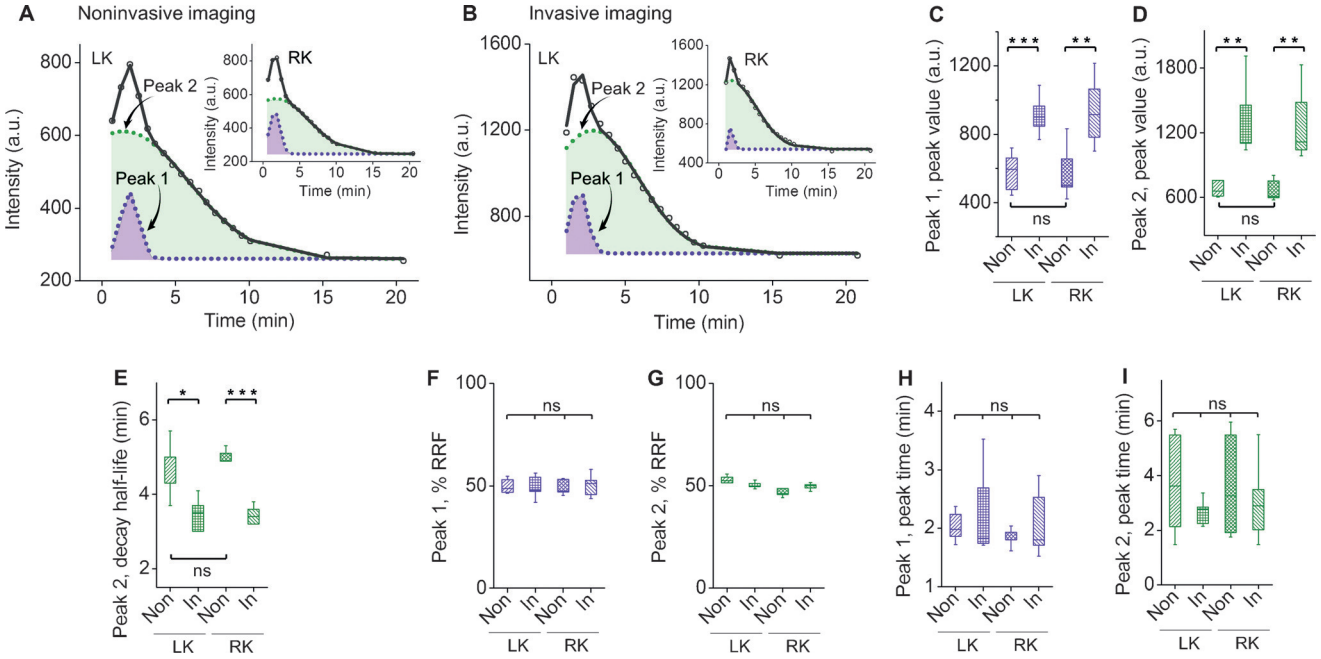

Figure 3. Quantitative comparison of noninvasive and invasive kidney imaging with GS-AuNPs. A, B) Representative time-fluorescence intensity curves (TFICs) of kidneys obtained from noninvasive (A) and invasive (B) imaging of the same mouse after GS-AuNPs injection (0–20 min). The curves (in black) can be deconvoluted to peak 1 and peak 2 (in purple and green, respectively). C–I) Statistical analysis of peak parameters extracted from noninvasive (Non) and invasive (In) kidney TFICs. The parameters included peak value (C, D), decay half-life (E), percentage of relative renal function (% RRF; F, G) and peak time (H, I), which are used to evaluate kidney function in clinical practice. LK, left kidney; RK, right kidney. $N = 6$ for C–I, mean ± s.d., $*P < 0.05$, $**P < 0.01$, $***P < 0.001$; ns, no significant difference.

obtained with GS-AuNPs is very close to the invasive one in profile: a rapid ascending segment in the fluorescence signal followed by a descending segment with two distinct decay kinetics (Figure 3 A,B). Further deconvolution of these kidney TFICs revealed two closely located peaks (peak 1 and 2), which were very similar to vascular phase and tubular phase as previously identified in kidney time-intensity curves of Gd-DTPA.[18]

To gain more quantitative understandings of the similarities and differences in kidney TFICs measured noninvasively and invasively after injection of GS-AuNPs, we extracted and compared some key parameters from the two peaks such as peak value, peak time, decay half-life and percentage of relative renal function (% RRF), which are often used in radiology-based kidney functional imaging.[19] Owing to the small light absorption of skin, the peak values detected in invasive imaging were slightly higher than those measured with noninvasive imaging (Figure 3 C,D). Furthermore, decay half-lives of peak 2 obtained from noninvasive imaging were just one minute longer than those from invasive imaging (Figure 3 E), dramatically different from those with IRDye 800CW (Figure 2 D). On the other hand, regarding % RRF ([peak value of peak 1 or 2/(peak value of peak 1 + peak value of peak 2)] × 100 %) and peak times, no significant differences were observed between noninvasive and invasive kidney TFICs (Figure 3 F–I). The LK and RK also exhibited no differences in all of the parameters tested (Figure 3 F–I and Table S1), consistent with the previous observations.[19] These results suggest that noninvasive kidney TFICs indeed reflect how the GS-AuNPs pass through the kidneys.

In summary, while NIR-emitting organic dyes meet the requirement on the light penetration depth for kidney imaging in small animals, their intrinsic large π-conjugation also induced rapid and persistent fluorescence background in the skin, making it highly challenging to noninvasively image KCK. With renal-clearable NIR-emitting GS-AuNPs, this long-standing challenge in noninvasive fluorescence kidney functional imaging can be addressed: we observed approximately 50- and 1000-fold increases in kidney-contrast enhancement and imaging time windows over IRDye 800CW because of their desired in vivo behaviors (low skin distribution, rapid clearance from the skin, high kidney accumulation, and long retention in the blood). As a result, high contrast noninvasive fluorescence imaging of KCK can be achieved, laying down a foundation for future fluorescence kidney functional imaging.

It should also be noted, low tissue penetration depth of the light, an intrinsic limitation of fluorescence imaging, will remain a roadblock for future clinical translation of these renal-clearable luminescent AuNPs in kidney functional imaging. One potential solution is to incorporate radioisotopes, such as ^{198}[Au] into these GS-AuNPs,[14] so that they can serve as radiotracers for single-photon emission computed tomography (SPECT) imaging of kidney function. The related studies will be reported in our future work.

Acknowledgements

This study was supported by the NIH (1R01DK103363), CPRIT (RP120588 and RP140544) and the start-up fund from the University of Texas at Dallas. We thank C. Mohan and Y. Du for discussions.

Keywords: fluorescence imaging · imaging agents · kidney clearance kinetics · nanoparticles · renal clearance

How to cite: *Angew. Chem. Int. Ed.* **2015**, *54*, 15434–15438
Angew. Chem. **2015**, *127*, 15654–15658

[1] a) R. A. Star, *Kidney Int.* **1998**, *54*, 1817–1831; b) L. S. Chawla, P. W. Eggers, R. A. Star, P. L. Kimmel, *N. Engl. J. Med.* **2014**, *371*, 58–66.

[2] a) A. T. Taylor, *J. Nucl. Med.* **2014**, *55*, 608–615; b) N. Grenier, F. Basseau, M. Ries, B. Tyndal, R. Jones, C. Moonen, *Abdom. Imaging* **2003**, *28*, 164–175; c) J. D. Krier, E. L. Ritman, Z. Bajzer, J. C. Romero, A. Lerman, L. O. Lerman, *Am. J. Physiol. Renal. Physiol.* **2001**, *281*, F630–F638.

[3] F. J. Penna, J. S. Chow, B. J. Minnillo, C. C. Passerotti, C. E. Barnewolt, S. T. Treves, F. H. Fahey, P. S. Dunning, D. A. Freilich, A. B. Retik, H. T. Nguyen, *J. Urol.* **2011**, *185*, 2405–2413.

[4] a) H. Hyun, M. H. Park, E. A. Owens, H. Wada, M. Henary, H. J. M. Handgraaf, A. L. Vahrmeijer, J. V. Frangioni, H. S. Choi, *Nat. Med.* **2015**, *21*, 192–197; b) H. S. Choi, S. L. Gibbs, J. H. Lee, S. H. Kim, Y. Ashitate, F. Liu, H. Hyun, G. Park, Y. Xie, S. Bae, M. Henary, J. V. Frangioni, *Nat. Biotechnol.* **2013**, *31*, 148–153; c) L. Cui, Q. Lin, C. S. Jin, W. Jiang, H. Huang, L. Ding, N. Muhanna, J. C. Irish, F. Wang, J. Chen, G. Zheng, *ACS Nano* **2015**, *9*, 4484–4495; d) S. D. Perrault, W. C. W. Chan, *Proc. Natl. Acad. Sci. USA* **2010**, *107*, 11194–11199; e) L. Q. Xiong, A. J. Shuhendler, J. H. Rao, *Nat. Commun.* **2012**, *3*, 1193; f) G. Hong, S. Diao, J. Chang, A. L. Antaris, C. Chen, B. Zhang, S. Zhao, D. N. Atochin, P. L. Huang, K. I. Andreasson, C. J. Kuo, H. Dai, *Nat. Photonics* **2014**, *8*, 723–730.

[5] S. Gioux, H. S. Choi, J. V. Frangioni, *Mol. Imaging* **2010**, *9*, 237–255.

[6] a) S. Tobis, J. K. Knopf, C. R. Silvers, J. Marshall, A. Cardin, R. W. Wood, J. E. Reeder, E. Erturk, R. Madeb, J. Yao, E. A. Singer, H. Rashid, G. Wu, E. Messing, D. Golijanin, *Urology* **2012**, *79*, 958–964; b) S. Tobis, J. Knopf, C. Silvers, J. Yao, H. Rashid, G. Wu, D. Golijanin, *J. Urol.* **2011**, *186*, 47–52.

[7] a) R. Kumar, I. Roy, T. Y. Ohulchanskky, L. A. Vathy, E. J. Bergey, M. Sajjad, P. N. Prasad, *ACS Nano* **2010**, *4*, 699–708; b) X. L. Zhang, Y. L. Tian, H. B. Zhang, A. Kavishwar, M. Lynes, A. L. Brownell, H. B. Sun, Y. H. Tseng, A. Moore, C. Z. Ran, *Sci. Rep.* **2015**, *5*, 13116; c) E. A. Sykes, Q. Dai, K. M. Tsoi, D. M. Hwang, W. C. W. Chan, *Nat. Commun.* **2014**, *5*, 3796.

[8] a) R. L. Sheridan, K. T. Schomaker, L. C. Lucchina, J. Hurley, L. M. Yin, R. G. Tompkins, M. Jerath, A. Torri, K. W. Greaves, D. P. Bua, *J. Burn Care Rehabil.* **1995**, *16*, 602–604; b) H. Ra, E. González-González, M. J. Uddin, B. L. King, A. Lee, I. Ali-Khan, L. J. Marnett, J. Y. Tang, C. H. Contag, *Neoplasia* **2015**, *17*, 201–207.

[9] C. K. Rowe, F. B. Franco, J. A. B. A. Barbosa, B. J. Minnillo, J. S. Chow, T. Treves, A. B. Retik, H. T. Nguyen, *J. Urol.* **2012**, *188*, 1978–1985.

[10] H. Hyun, E. A. Owens, H. Wada, A. Levitz, G. Park, M. H. Park, J. V. Frangioni, M. Henary, H. S. Choi, *Angew. Chem. Int. Ed.* **2015**, *54*, 8648–8652; *Angew. Chem.* **2015**, *127*, 8772–8776.

[11] a) X. H. Gao, Y. Y. Cui, R. M. Levenson, L. W. K. Chung, S. M. Nie, *Nat. Biotechnol.* **2004**, *22*, 969–976; b) R. Jin, *Nanoscale* **2010**, *2*, 343–362; c) C. V. Conroy, J. Jiang, C. Zhang, T. Ahuja, Z. H. Tang, C. A. Prickett, J. J. Yang, G. L. Wang, *Nanoscale* **2014**, *6*, 7416–7423; d) J. Zheng, C. Zhou, M. Yu, J. Liu, *Nanoscale* **2012**, *4*, 4073–4083.

[12] a) H. S. Choi, W. Liu, P. Misra, E. Tanaka, J. P. Zimmer, B. I. Ipe, M. G. Bawendi, J. V. Frangioni, *Nat. Biotechnol.* **2007**, *25*, 1165–1170; b) A. A. Burns, J. Vider, H. Ow, E. Herz, O. Penate-Medina, M. Baumgart, S. M. Larson, U. Wiesner, M. Bradbury, *Nano Lett.* **2009**, *9*, 442–448; c) H. Chen, G. D. Wang, W. Tang, T. Todd, Z. Zhen, C. Tsang, K. Hekmatyar, T. Cowger, R. B. Hubbard, W. Zhang, J. Stickney, B. Shen, J. Xie, *Adv. Mater.* **2014**, *26*, 6761–6766; d) S. Tang, M. Chen, N. Zheng, *Small* **2014**, *10*, 3139–3144; e) M. Yu, J. Zheng, *ACS Nano* **2015**, *9*, 6655–6674.

[13] C. Zhou, M. Long, Y. Qin, X. Sun, J. Zheng, *Angew. Chem. Int. Ed.* **2011**, *50*, 3168–3172; *Angew. Chem.* **2011**, *123*, 3226–3230.

[14] C. Zhou, G. Y. Hao, P. Thomas, J. B. Liu, M. X. Yu, S. S. Sun, O. K. Oz, X. K. Sun, J. Zheng, *Angew. Chem. Int. Ed.* **2012**, *51*, 10118–10122; *Angew. Chem.* **2012**, *124*, 10265–10269.

[15] M. Yu, C. Zhou, J. Liu, J. D. Hankins, J. Zheng, *J. Am. Chem. Soc.* **2011**, *133*, 11014–11017.

[16] J. Liu, M. Yu, C. Zhou, S. Yang, X. Ning, J. Zheng, *J. Am. Chem. Soc.* **2013**, *135*, 4978–4981.

[17] J. E. Hall, *Guyton and Hall Textbook of Medical Physiology*, 12th ed., Saunders Elsevier, Philadelphia, **2011**, p. 304.

[18] *Radiological imaging of the kidney*, 1st ed., Springer, Berlin, Heidelberg, **2011**, p. 849.

[19] a) G. Hao, Y. Du, X. J. Zhou, J. Guo, X. Sun, C. Mohan, O. K. Oez, *PLoS One* **2013**, *8*, e57418; b) J. Roberts, B. Chen, L. M. Curtis, A. Agarwal, P. W. Sanders, K. R. Zinn, *Am. J. Physiol. Renal. Physiol.* **2007**, *293*, F1408–F1412; c) M. N. Tantawy, R. Jiang, F. Wang, K. Takahashi, T. E. Peterson, D. Zemel, C. M. Hao, H. Fujita, R. C. Harris, C. C. Quarles, T. Takahashi, *BMC Nephrol.* **2012**, *13*, 168.

Received: August 22, 2015
Revised: October 13, 2015
Published online: October 29, 2015

